HHS Public Access

Author manuscript

Clin Nucl Med. Author manuscript; available in PMC 2019 January 04.

Published in final edited form as:

Clin Nucl Med. 2015 January ; 40(1): 1–8. doi:10.1097/RLU.0000000000000611.

Simultaneous Whole-Body Time-of-Flight ^{18}F-FDG PET/MRI:

A Pilot Study Comparing SUV_{max} With PET/CT and Assessment of MR Image Quality

Andrei Iagaru, MD[*], **Erik Mittra, MD, PhD**[*], **Ryogo Minamimoto, MD**[*], **Mehran Jamali, MD**[*], **Craig Levin, PhD**[†], **Andrew Quon, MD**[*], **Garry Gold, MD**[‡], **Robert Herfkens, MD**[‡], **Shreyas Vasanawala, MD, PhD**[‡], **Sanjiv Sam Gambhir, MD, PhD**[§], and **Greg Zaharchuk, MD, PhD**[‡]

[*]Division of Nuclear Medicine and Molecular Imaging, Stanford University Medical Center

[†]Stanford University Medical Center, Molecular Imaging Program at Stanford (MIPS)

[‡]Stanford University Medical Center, Department of Radiology

[§]Stanford University Medical Center, Departments of Radiology, Bio-engineering, Materials Science and Engineering, Molecular Imaging Program at Stanford (MIPS), Stanford, CA

Abstract

Purpose: The recent introduction of hybrid PET/MRI scanners in clinical practice has shown promising initial results for several clinical scenarios. However, the first generation of combined PET/MRI lacks time-of-flight (TOF) technology. Here we report the results of the first patients to be scanned on a completely novel fully integrated PET/MRI scanner with TOF.

Materials and Methods: We analyzed data from patients who underwent a clinically indicated ^{18}F FDG PET/CT, followed by PET/MRI. Maximum standardized uptake values (SUV_{max}) were measured from ^{18}F FDG PET/MRI and ^{18}F FDG PET/CT for lesions, cerebellum, salivary glands, lungs, aortic arch, liver, spleen, skeletal muscle, and fat. Two experienced radiologists independently reviewed the MR data for image quality.

Results: Thirty-six patients (19 men, 17 women, mean [±standard deviation] age of 61 ± 14 years [range: 27–86 years]) with a total of 69 discrete lesions met the inclusion criteria. PET/CT images were acquired at a mean (±standard deviation) of 74 ± 14 minutes (range: 49–100 minutes) after injection of 10 ± 1 mCi (range: 8–12 mCi) of ^{18}F FDG. PET/MRI scans started at 161 ± 29 minutes (range: 117 – 286 minutes) after the ^{18}F FDG injection. All lesions identified on PET from PET/CT were also seen on PET from PET/MRI. The mean SUV_{max} values were higher from PET/MRI than PET/CT for all lesions. No degradation of MR image quality was observed.

Conclusion: The data obtained so far using this investigational PET/MR system have shown that the TOF PET system is capable of excellent performance during simultaneous PET/MR with routine pulse sequences. MR imaging was not compromised. Comparison of the PET images from PET/CT and PET/MRI show no loss of image quality for the latter. These results support further investigation of this novel fully integrated TOF PET/MRI instrument.

Andrei Iagaru, MD, Division of Nuclear Medicine and Molecular Imaging, Stanford University Medical Center, 300 Pasteur Dr, Room H-0101, Stanford, CA 94305 USA. aiagaru@stanford.edu.

Conflicts of interest and sources of funding: none declared.

Keywords

PET; CT; MRI; TOF; simultaneous

More than a decade ago, multimodality imaging was introduced into routine clinical practice with the development of the PET/CT. Since then, PET/CT has been widely accepted in clinical imaging and has emerged as one of the main cancer imaging modalities. The recent introduction of hybrid PET/MRI scanners in clinical practice[1–3] showed promising initial results for several clinical scenarios.[4,5] The combination of functional information delivered by PET with the morphologic and functional imaging of MR imaging (e.g., diffusion-weighted imaging, dynamic contrast-enhanced MR imaging and MR spectroscopy) offers exciting possibilities for clinical applications as well as basic research.

However, the differences between CT and MR imaging are fundamental. This leads to distinct differences between PET/CT and PET/MRI not only regarding image interpretation but also concerning data acquisition, data processing, and image reconstruction. PET/MRI is expected to show advantages over PET/CT in clinical applications in which MRI is known to be superior to CT due to its high intrinsic soft tissue contrast, such as in the brain, neck, and pelvis. However, as of now, only assumptions can be made about the future clinical role of PET/MRI, as data about the performance of PET/MRI in the clinical setting are still relatively limited.[6]

A novel, integrated whole-body PET/MRI scanner with time of flight (TOF) capability was recently installed at our institution. Therefore, we were prompted in this pilot stuyd to determine if ^{18}F FDG PET/CT and ^{18}F FDG PET/MRI provide equivalent results for evaluation of patients and explore any possible differences in semi-quantitative parameters such as SUV_{max}.

PATIENTS AND METHODS

Clinical Study

The local Institutional Review Board approved the protocol. Written informed consent was obtained from each patient. Participants referred for oncological standard of care ^{18}F FDG PET/CT were recruited between January – July 2014. The clinical ^{18}F FDG PET/CT was done first, followed by PET/MRI with only a single FDG injection. All women of childbearing age who were not surgically sterile had a urine pregnancy test prior to the PET/MRI. All patients were screened for the presence of metallic implants or other contradictions to MRI, including claustrophobia.

PET/CT Imaging

The PET/CT scans were acquired using a standard clinical protocol after injection of a prescribed dose of 10 mCi of ^{18}F FDG.[7] The patients fasted at least 6 hours prior to the scans and blood glucose levels were less than 150 mg/dl at the time of ^{18}F FDG injection. The participants were scanned in 3D mode on a GE Discovery 600 PET/CT (10 patients) or a GE Discovery 690 PET/CT (26 patients). The latter system has TOF capability, but with a

significantly lower time resolution compared to the PET in the PET/MR system studied. Our imaging protocol requires a BMI>25 for TOF acquisition. Fifteen of the patients had a BMI>25; therefore, TOF data was acquired and reconstructed only in these 15 patients. First, a CT scan (5 mm contiguous axial cuts) was obtained from the skull base to the mid-thighs for oncology patients. The acquisition was obtained in helical mode, using 140 kV, 40 mAs and a 512 × 512 matrix size. The CT scan was used for attenuation correction purposes and to help in anatomic localization of ^{18}F FDG. Immediately after the CT, an emission PET scan was acquired over the same anatomical regions. The acquisition time was 3 minutes per bed position (47 slices/bed) in 6 beds with 11-slice overlap at the edge of the axial field of view. The PET emission scan was corrected using attenuation data of the CT scan. PET images were reconstructed using ordered subset expectation maximization (OSEM) with 2 iterations and 32 subsets for Discovery 600 or 2 iterations and 24 subsets for Discovery 690, then reviewed and analyzed using Advantage Workstation (GE Healthcare, WI, USA).

PET/MRI Imaging

The silicon photomultiplier (SiPM)-based TOF PET system technology was developed by GE Healthcare, based on a modified GE Discovery 750w 3 T MR scanner. Key design parameters of the GE TOF Discovery PET/MRI scanner have been previously reported.[8] Notably the time resolution is better than that offered by the PET/CT system studied. Immediately after completion of the PET/CT exam, the patients were transferred to the PET/MRI suite and underwent the PET/MRI image acquisition. Acquisition began at the vertex and moved toward the pelvic region. The combined PET/MRI acquisition was initiated with 3–5 table positions with 4 min acquisition time per table position. A 2-point Dixon 3-dimensional volumetric interpolated T1-weighted fast spoiled gradient echo image MR sequence (TR/TE1/TE2: 4.1/1.1/2.2 ms; FOV 50 × 37.5 cm; matrix 256 × 128; slice thickness/overlap: 5.2/2.6 mm; 120 images/slab; imaging time 18 sec) reconstructed in the axial plane was acquired at each table position and used to generate attenuation maps and for anatomic registration of the PET results. PET images were reconstructed using OSEM with 2 iterations and 28 subsets. Simultaneously with the start of the Dixon MRI sequence, the PET acquisition started at the same table position, thus ensuring optimal temporal and regional correspondence between MRI and PET data.

First a 3D, T1-weighted LAVA-Flex protocol was acquired for MR-based attenuation correction (MRAC) using four sets of MRI images: WATER, FAT, InPhase, OutPhase. The images are segmented into different tissue types, using segmentation parameters that take account of the anatomy. Thus, for example, air pockets in the abdomen are treated differently than air in the lungs. There are two additional special cases: the head, and the arms. The head is registered to an atlas, and from this atlas is derived the approximate location and size of the bones in the skull, as well as air cavities. The arms, and generally those parts of the body that are outside of the central FOV of the MRI system, need special treatment as well. To make up for the lack of MR information, the PET data is reconstructed using TOF information, but without attenuation information. The resulting image shows a fairly clear delineation of the skin line thanks to the excellent timing resolution of the PET detector. Based on this outline, the attenuation map is filled with “soft tissue” for those regions for which no good MR data is available. Outside of the head, bone is not segmented

separately; instead it is given the attenuation properties of soft tissue. The result of all of the above is an attenuation correction that produces good results over a range of patient sizes and anatomies.

Additional sequences were acquired in the coronal plane as follows: short tau inversion recovery (STIR) images (TR/TI/TE: 4300/190/44.2 ms; FOV 44–46 cm; matrix 384 × 224; slice thickness/skip: 8/0 mm; 22–38 slices depending on size; 2 nex; acceleration factor 2; imaging time 1:52 – 7:11 min) and 3D spoiled gradient echo liver acquisition with volume acqusition (LAVA) images (TR/TE1/TE2: 4.9/1.3/2.5 ms; FOV 44 cm; matrix 320 × 224; slice thickness/overlap: 4/2 mm; 88–152 slices depending on size; 2 nex; acceleration factor 2; imaging time 0:21 – 0:55 min), which allowed for water and fat separation, were acquired in each alternating bed position (e.g., 1, 3, 5, etc.). Because of the large FOV this allow coverage of both the current and subsequent bed position, such that a full body image could be created from these sequences. In the thorax region, the MRI scans were acquired during breath-hold in shallow inspiration, similarly to the acquisition of the low-dose CT.[9] Images were reviewed and analyzed with the software provided by the manufacturer (Advantage Workstation).

Image Analysis

Image interpretation of the ^{18}F FDG PET from PET/CT and PET/MRI scans was done in randomized order by two board-certified Nuclear Medicine physicians (AI, ESM) blinded to the diagnosis and the results of other imaging studies. Maximum standardized uptake values (SUV_{max}) were recorded by one reader (AI) for all the detected lesions and normal tissues (cerebellum, parotid gland, aortic arch, normal lung, liver, spleen, gluteal muscle and gluteal fat). Two board-certified Radiologists (GZ, SV) reviewed the MRI data for image quality. Discrepancies were resolved by consensus read, with a third reader as referee if needed (GG, RH, AQ, SSG).

Statistical Analysis

Paired two-sample t-test using GraphPad (GraphPad Software, San Diego, CA) were done to compare the SUV_{max} data from normal tissues and lesions between PET from PET/CT and PET from PET/MRI. A P- value of <0.05 was considered significant.

RESULTS

Thirty-six patients were enrolled in the study (19men, 17women). The participants had a mean (±standard deviation [SD]) age of 61 ± 14 years (range: 27–86 years). Eight percent of the participants were referred for initial treatment strategy (formerly diagnosis and initial staging), while 92% of them were referred for subsequent treatment strategy (includes treatment monitoring, restaging and detection of suspected recurrence), based on the National Coverage Determination for ^{18}F FDG PET for Oncologic Conditions from the Centers for Medicare & Medicaid Services.[10] The participants' clinical characteristics are presented in Table 1.

PET/CT images were acquired at a mean (±SD) of 73 ± 14 minutes (range: 49–100 minutes) after injection of 10 ± 1 mCi (range: 8–12 mCi) of ^{18}F FDG. Variations in doses and times

from injection to imaging are part of routine clinical practice, including major academic centers.[10] PET/MRI scans started at 161 ± 29 minutes (range: 117–286 minutes) after the ^{18}F FDG injection, a delay related to the time of PET/CT acquisition and the physical location of the PET/MRI scanner in relation to the PET/CT scanners. The time to complete these oncologic PET/MRI cases was 51 ± 14 min. Three patients did not complete the entire PET/MRI examination due to delays related to problems with the early version of the acquisition software. Therefore, 2 patients only received the head & neck acquisition of the PET/MRI and 1 patient only received the head & neck and chest acquisition of the PET/MRI.

Eleven of the 36 patients had no abnormal uptake on either PET from PET/CT or PET/MRI. More lymph nodes were seen on PET from PET/MRI than on PET from PET/CT in 5 participants. A similar finding was noted for lung nodules in 3 patients. A brain lesion was better evaluated on PET/MRI than on PET/CT. No lesions were more numerous on PET from PET/CT than on PET from PET/MRI. Representative PET images from PET/CT and PET/MRI, as well as corresponding MRI images are shown as Figures 1–4.

MRI Image Quality

MRI images were graded using a 0–3 scale (0 = severe artifacts, not diagnostic; 1 = moderate artifacts, minimally diagnostic; 2 = mild artifacts, reasonably diagnostic; 3 = no artifacts, diagnostic). For these MRI images, 29/36 were scored 3, another 6/36 were scored 2, and 1/36 was scored 1. The primary cause of the artifacts was motion.

SUV_{max} Values in Normal Tissues and Lesions

The mean SUV_{max} values were lower on PET/MRI compared with PET/CT for all evaluated normal tissues, except for parotid gland and gluteal muscle. These changes for all regions in all patients had a mean (±SD) of –14% ± 22 (range: –47% to 23%) and were statistically significant for all tissues analyzed except gluteal fat, as shown in Table 2.

On a per lesion analysis, a total of 69 lesions were identified in 25 of the 36 patients scanned. These included 38 lymph nodes, 9 lung nodules, 8 bone lesions and 14 other lesions (3 thyroid nodules, 3 soft tissue lesions, 2 colorectal lesions, 2 mediastinal masses, 2 liver lesions, 1 tonsillar mass, 1 brain lesion). The SUV_{max} values for all lesions were 21 ± 25% (range: –48% to 99%) higher on PET/MRI (TOF) compared with PET/CT (non-TOF), regardless of whether the PET/CT scan was done using the Discovery 600 or 690 scanner (Table 4). These SUV_{max} increases are expected after the additional uptake time.[11] The changes were statistically significant for analyses done separately for all lesions, lymph nodes, lung nodules and other lesions, but not for the bone lesions (Table 3). There were statistically significant differences in the measurements of SUV_{max} values in 26 lesions when analysing the TOF vs non-TOF data from the 15 patients scanned using TOF on the Discovery 690 scanner, except for a statistically significant difference in SUV_{max} values for lung nodules (n = 5; P: 0.04). However, there was a trend toward significance when analyzing TOF and non-TOF data from PET/CT vs. PET/MRI. These comparisons of TOF vs. non-TOF data from 15 patients are shown in Table 4. Kershah et al. and Heusch et al. also reported similar differences between MR attenuation correction vs. CT attenuation

correction derived SUV values and they were attributed to the time-delay between the PET/CT and PET/MRI scans or biologic clearance of radiotracer.[12,13]

We also analyzed the ratios of uptake in lesions (n = 69) and various backgrounds (aortic arch, liver and cerebellum). The mean (±SD) for the lesion:aortic arch ratios were 3.7 ± 4.0 (range: 0.7–21.6) for PET/CT (non-TOF) and 7.4 ± 7.5 (range: 1.4–44.8) for PET/MRI (TOF) (P value: 0.0001); for lesion:liver ratios the values were 2.0 ± 1.7 (range: 0.4–9.5) for PET/CT (non-TOF) and 3.2 ± 2.7 (range: 0.6–17.1) for PET/MRI (TOF) (P value: 0.0001); for lesion:cerebellum ratios the values were 0.6 ± 0.4 (range: 0.1–2.3) for PET/CT (non-TOF) and were 0.8 ± 0.5 (range: 0.1–3.1) for PET/MRI (TOF) (P value: 0.0001). The same analysis of the data from TOF PET/CT lesions (n = 26) produced the results described below. The mean (±SD) for the lesion:aortic arch ratios were 4.7 ± 3.6 (range: 1.3–14.1) for PET/CT (TOF) and 11.1 ± 10.3 (range: 3.2–44.8) for PET/MRI (TOF) (P value: 0.0001); for lesion:liver ratios the values were 2.5 ± 1.6 (range: 0.9–6.8) for PET/CT (TOF) and 3.8 ± 2.8 (range: 1.0–12.1) for PET/MRI (TOF) (P value: 0.0001); for lesion:cerebellum ratios the values were 0.8 ± 0.4 (range: 0.3–1.9) for PET/CT (TOF) and were 0.9 ± 0.6 (range: 0.3–3.1) for PET/MRI (TOF) (P value: 0.0036).

Radiation Dose

Using a dose relationship of 1.1 mSv/mCi for the ^{18} F FDG component of PET/CT,[14] the radiation exposure from the injected dosage of radiopharmaceutical had a mean (±SD) of 11 ± 1 mSv (range: 9–13 mSv), which is also the total radiation exposure for the PET/MR studies. The CT radiation dose received by the patients in this cohort was calculated from the reported DLP and had a mean (±SD) of 6 ± 3 mSv (range: 1–15 mSv). Therefore, the total radiation exposure from ^{18}F FDG PET/CT had a mean (±SD) of 17 ± 3 mSv (range: 11–25 mSv). This data is shown in Table 5.

DISCUSSION

In the current study we have shown that TOF simultaneous PET/MRI is feasible and produces results that are comparable with PET/CT. Despite acquiring the images over 2 hours after ^{18}F FDG injection, no findings from PET/CT were missed on PET/MRI. Due to the combination of high photon sensitivity, TOF, and relatively long delay post-injection, high quality images with very low background were achieved with the PET/MR studies.

Two architectures of combined PET/MRI have been manufactured: a) tandem systems, with the PET and MR systems located either in different rooms with a dockable table[15] or in the same room,[2] and b) integrated systems, with the PET and MR systems built concentrically within a single gantry.[16] The tandem systems allow minimal interference between the two systems and thus only require minor changes in the PET and MR components. The integrated systems require a completely new architecture and technology, but allow truly simultaneous acquisitions. The major challenge when PET and MR data are acquired simultaneously lies in the fact that the photomultiplier tubes traditionally used in PET to read the light output of the scintillation crystals cannot be operated within a strong magnetic field. Tandem systems avoid this issue through the physical separation of the scanners and suitable shielding of the components. Truly integrated systems have been enabled by the

creation of PET detectors based on solid state (semiconductor) photosensors that are much less sensitive to magnetic fields. Early systems used Avalanche Photodiodes (APDs). The newer Silicon Photomultiplier (SiPM) technology applied in the system described here has the advantage of providing excellent timing resolution, giving the system TOF PET capability.

Although clinical applications were obvious at the time of the introduction of the first PET/CT scanner[17] and have completely replaced stand-alone PET in oncology, clinical applications of PET/MRI are currently not clearly defined. This is in part due to the lack of clinical data, although some groups that installed PET/MRI worldwide have started to report such data.[18–21] Preliminary results suggest that PET/MRI may have advantages over PET/CT in oncology, for applications such as head and neck, prostate and musculoskeletal imaging. In liver imaging, more PET-positive lesions are seen on MRI than on CT.[22] Brain imaging may be an important domain for PET/MRI, particularly in dementia and neuro-oncological evaluation. The role of PET/MR in the cardiovascular system is preliminary, with initial studies demonstrating feasibility.[23,24]

PET/MRI may be preferred over PET/CT where the unique features of MRI provide more robust imaging evaluation. The exact role and potential utility of simultaneous data acquisition in specific research and clinical settings will need to be defined. It may be that simultaneous PET/MRI will be best suited for clinical situations that are disease-specific, organ-specific, related to pediatric diseases, or in patients undergoing repeated imaging.[25] Horsch and colleagues reported that the effective dose of a PET/MRI scan was reduced by 80% compared with that of the equivalent PET/CT examination in their study of pediatric patients.[26] Based on the results of our study, total radiation dose can be reduced by 30% simply from replacing CT with MRI. However, since the protocol requires to image for longer per bed position for the PET/MRI and the new PET detector system is approximately three times more sensitive than current GE PET systems, one can envision further reducing the radiation exposure by reducing the injected radiopharmaceutical dose by 50% while achieving the same PET image quality as with conventional PET/CT scanners. Future studies will have to further evaluate this potential benefit.

Currently, it is not clear where the simultaneity afforded by a fully integrated PET/MRI is really needed. With the increasing installed base of systems, clinical data will be forthcoming and define more clearly where there is clinical value in PET/MR, including simultaneous PET/MR. The clinical use of novel PET tracers for biological processes such as angiogenesis, lipids, glutamate or other specific metabolic pathways may require the simultaneous information from PET and functional MRI.

Our pilot study is limited by the low number of participants and lesions included, as well as by the order of imaging. Future studies including larger number of patients are needed to fully evaluate the appropriate clinical indications for simultaneous TOF PET/MRI scanners compared to PET/CT. Also ideally, PET/CT and PET/MRI should have been done in randomized order. However, this was not possible due to regulatory constraints. In future routine clinical practice, PET/MRI will likely be performed at shorter delays from radiotracer injection than in this study, and PET image quality and its characteristics will

differ. Another limitation of the study is that the patients were scanned on two separate PET/CT scanners, one of which had TOF capability; despite the fact that no significant difference was seen between the PET/CT scanners, this increased the variability of the study and also raises concern that many of the reported findings reflect only differences among the PET scanners, independent of hybrid imaging configuration.

CONCLUSION

The data obtained so far using this investigational PET/MR system have shown that the TOF PET system is capable of excellent performance during simultaneous PET/MR with routine pulse sequences. Importantly, MR imaging was not compromised. Comparison of the PET images from PET/CT and PET/MRI show no loss of image quality for the latter.

REFERENCES

1. Pichler B, Judenhofer M, Wehrl H. PET/MRI hybrid imaging: devices and initial results. European radiology. 2008;18:1077–1086. [PubMed: 18357456]
2. Zaidi H, Ojha N, Morich M, et al. Design and performance evaluation of a whole-body Ingenuity TF PET-MRI system. Physics in medicine and biology. 2011;56: 3091–3106. [PubMed: 21508443]
3. Boss A, Bisdas S, Kolb A, et al. Hybrid PET/MRI of Intracranial Masses: Initial Experiences and Comparison to PET/CT. Journal of Nuclear Medicine. 2010;51: 1198–1205. [PubMed: 20660388]
4. Miese F, Scherer A, Ostendorf B, et al. Hybrid (18)F-FDG PET-MRI of the hand in rheumatoid arthritis: initial results. Clinical rheumatology.2011;30:1247–1250. [PubMed: 21590292]
5. Boss A, Stegger L, Bisdas S, et al. Feasibility of simultaneous PET/MR imaging in the head and upper neck area. European radiology. 2011;21:1439–1446. [PubMed: 21308378]
6. Gaertner F, Fürst S, Schwaiger M. PET/MR: a paradigm shift. Cancer imaging. 2013;13:36–52. [PubMed: 23446110]
7. Delbeke D, Coleman RE, Guiberteau MJ, et al. Procedure Guideline for Tumor Imaging with 18F-FDG PET/CT 1.0. Journal of Nuclear Medicine. 2006;47:885–895. [PubMed: 16644760]
8. Levin C, Deller T, Peterson W, et al. Initial results of simultaneous whole-body ToF PET/MR. J NUCL MED MEETING ABSTRACTS. 2014;55:660.
9. Drzezga A, Souvatzoglou M, Eiber M, et al. First Clinical Experience with Integrated Whole-Body PET/MR: Comparison to PET/CT in Patients with Oncologic Diagnoses. Journal of Nuclear Medicine. 2012;53:845–855. [PubMed: 22534830]
10. Graham MM, Badawi RD, Wahl RL. Variations in PET/CT Methodology for Oncologic Imaging at U.S. Academic Medical Centers: An Imaging Response Assessment Team Survey. Journal of Nuclear Medicine. 2011;52:311–317. [PubMed: 21233185]
11. Cheng G, Torigian DA, Zhuang H, et al. When should we recommend use of dual time-point and delayed time-point imaging techniques in FDG PET? Eur J Nucl Med Mol Imaging. 2013;40:779–787. [PubMed: 23361859]
12. Kershah S, Partovi S, Traughber B, et al. Comparison of Standardized Uptake Values in Normal Structures Between PET/CT and PET/MRI in an Oncology Patient Population. Molecular Imaging and Biology. 2013;15:776–785. [PubMed: 23632951]
13. Heusch P, Buchbender C, Beiderwellen K, et al. Standardized uptake values for [18F] FDG in normal organ tissues: Comparison of whole-body PET/CT and PET/MRI. European Journal of Radiology. 2013;82:870–876. [PubMed: 23394765]
14. Jones SC, Alavi A, Christman D, et al. The Radiation Dosimetry of 2-[F-18]Fluoro-2-Deoxy-D-Glucose in Man. Journal of Nuclear Medicine. 1982;23:613–617. [PubMed: 6979616]
15. Kuhn FP, Crook DW, Mader CE, et al. Discrimination and anatomical mapping of PET-positive lesions: comparison of CT attenuation-corrected PET images with coregistered MR and CT images in the abdomen. Eur J Nucl Med Mol Imaging. 2013;40:44–51. [PubMed: 22955547]

16. Delso G, Fürst S, Jakoby B, et al. Performance Measurements of the Siemens mMR Integrated Whole-Body PET/MR Scanner. Journal of Nuclear Medicine. 2011;52:1914–1922. [PubMed: 22080447]
17. Townsend DW, Beyer T. A combined PET/CT scanner: the path to true image fusion. Br J Radiol. 2002;75Spec No:S24–S30. [PubMed: 12519732]
18. Kubiessa K, Purz S, Gawlitza M, et al. Initial clinical results of simultaneous 18F-FDG PET/MRI in comparison to 18F-FDG PET/CT in patients with head and neck cancer. European Journal of Nuclear Medicine and Molecular Imaging. 2014;41:639–648. [PubMed: 24292211]
19. Wetter A, Lipponer C, Nensa F, et al. Evaluation of the PET component of simultaneous [(18)F]choline PET/MRI in prostate cancer: comparison with [(18)F]choline PET/CT. Eur J Nucl Med Mol Imaging. 2014;41:79–88. [PubMed: 24085502]
20. Heusch P, Buchbender C, Kohler J, et al. Correlation of the apparent diffusion coefficient (ADC) with the standardized uptake value (SUV) in hybrid 18F-FDG PET/MRI in non-small cell lung cancer (NSCLC) lesions: initial results. Rofo. 2013;185:1056–1062. [PubMed: 23860802]
21. Chandarana H, Heacock L, Rakheja R, et al. Pulmonary nodules in patients with primary malignancy: comparison of hybrid PET/MR and PET/CT imaging. Radiology. 2013;268:874–881. [PubMed: 23737537]
22. Beiderwellen KJ, Poeppel TD, Hartung-Knemeyer V, et al. Simultaneous 68Ga-DOTATOC PET/MRI in patients with gastroenteropancreatic neuroendocrine tumors: initial results. Invest Radiol. 2013;48:273–279. [PubMed: 23493121]
23. Ripa RS, Knudsen A, Hag AM, et al. Feasibility of simultaneous PET/MR of the carotid artery: first clinical experience and comparison to PET/CT. Am J Nucl Med Mol Imaging. 2013;3:361–371. [PubMed: 23900769]
24. Petibon Y, Ouyang J, Zhu X, et al. Cardiac motion compensation and resolution modeling in simultaneous PET-MR: a cardiac lesion detection study. Phys Med Biol. 2013;58:2085–2102. [PubMed: 23470288]
25. Jadvar H, Colletti PM. Competitive advantage of PET/MRI. Eur J Radiol. 2014; 83:84–94. [PubMed: 23791129]
26. Hirsch F, Sattler B, Sorge I, et al. PET/MR in children. Initial clinical experience in paediatric oncology using an integrated PET/MR scanner. Pediatric Radiology. 2013;43:860–875. [PubMed: 23306377]

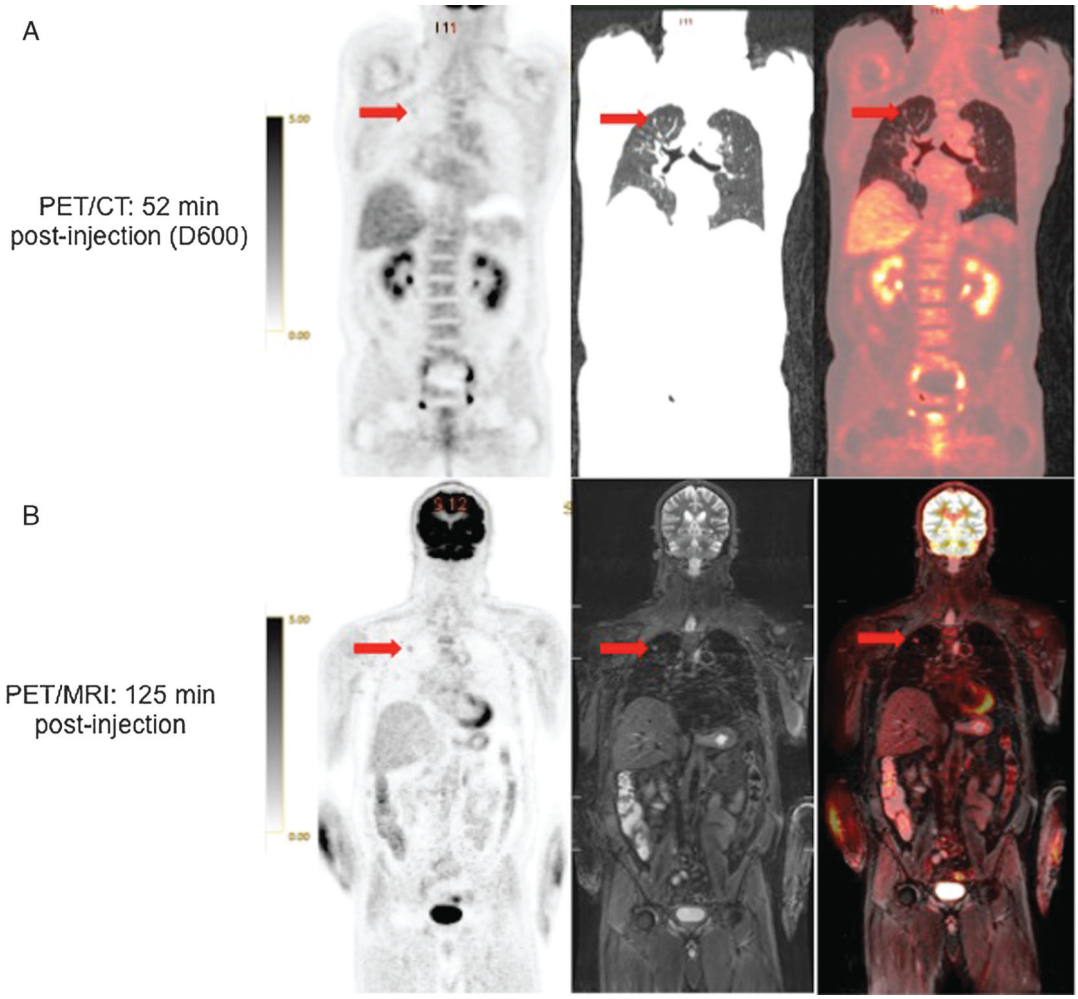

FIGURE 1.

52 year-old man with remote history of prostate cancer and newly diagnosed abdominal lymphoma. ^{18}F FDG-avid right upper lung nodule (arrow) is less conspicuous on PET from PET/CT (A) than on PET from PET/MRI (B). Coronal CT and STIR MR images also show the nodule (right). Fused PET/CT and PET/MRI images are also presented.

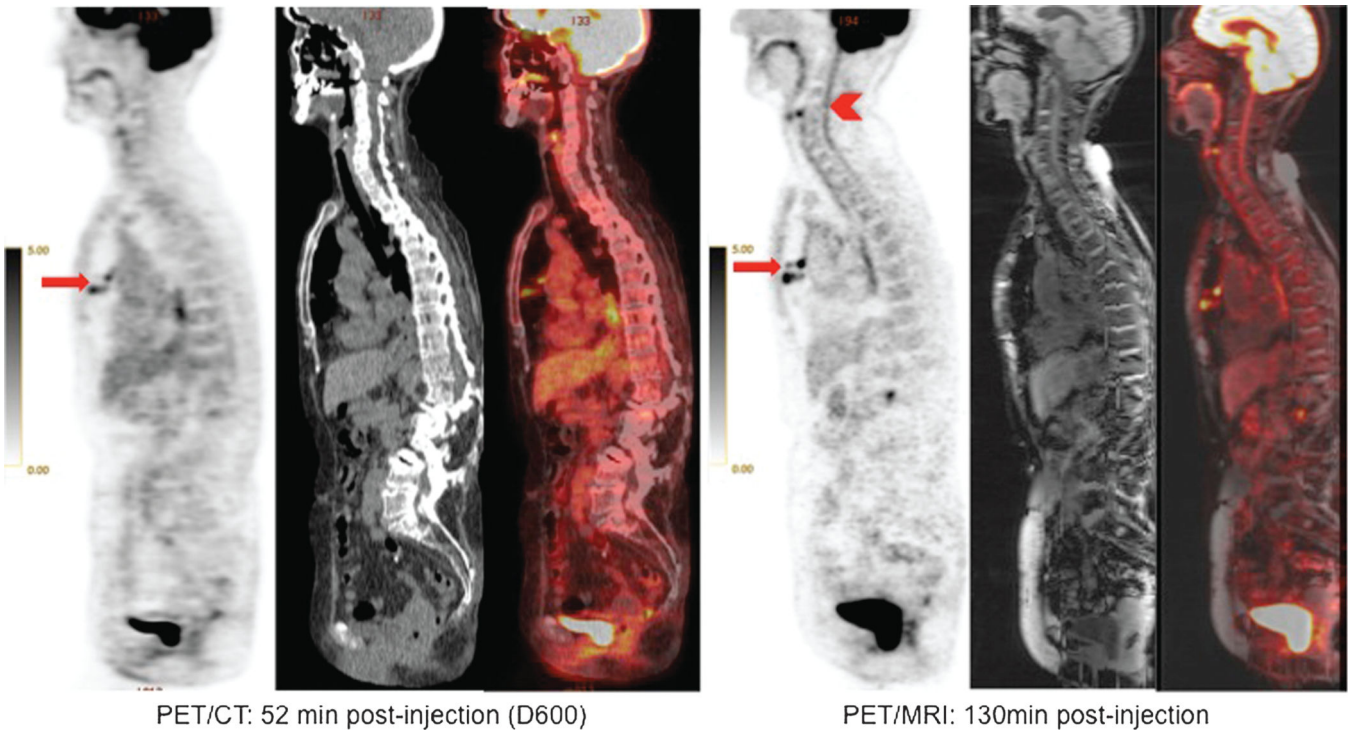

FIGURE 2.

79 year-old woman with lymphoma. ^{18}F FDG-avid mediastinal lymph nodes (arrows) are less conspicuous on PET from PET/CT than on PET from PET/MRI. High definition of spinal cord (arrowhead) is seen on PET from PET/MRI.

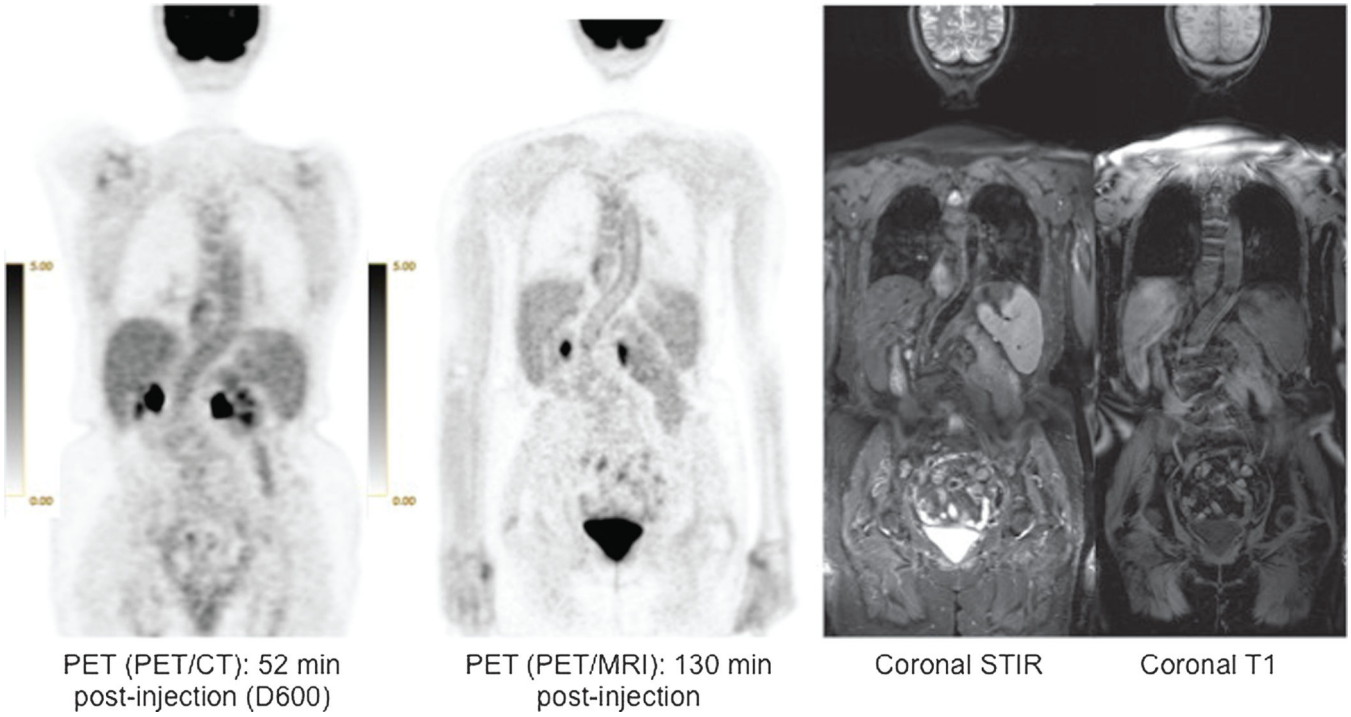

FIGURE 3.

79 year-old woman with lymphoma. High definition of thoracic and abdominal aortic walls (arrows) is noted on PET from PET/MRI. Corresponding coronal STIR and T1 MR images are also shown.

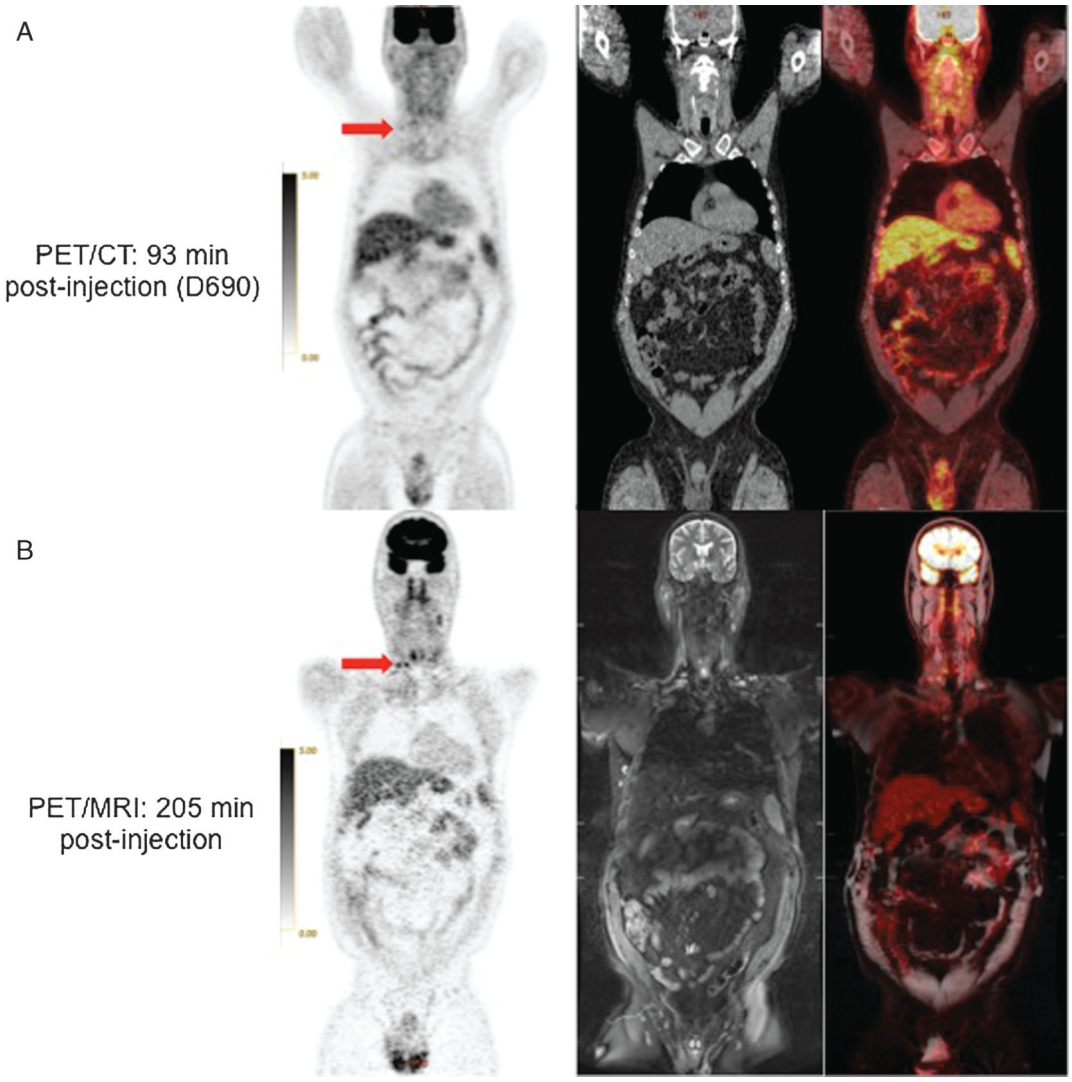

FIGURE 4.

64 year-old man with CLL. ^{18}F FDG-avid cervical lymph nodes (arrows) are less conspicuous on PET from PET/CT (A) than on PET from PET/MRI (B). Corresponding coronal CT, STIR MRI and fused PET/CT and PET/MR images are also shown.

TABLE 1.

Clinical Data About the Studied Participants

Age	Sex	Cancer	Indication	Stage	Treatment
70	M	Melanoma	Subsequent treatment strategy	IV	Surgery, chemo
75	F	NHL	Subsequent treatment strategy	III	Chemo
69	F	HD	Initial treatment strategy	III	None
66	M	Prostate	Subsequent treatment strategy	II	RT
79	F	NHL	Subsequent treatment strategy	IV	Chemo, RT
64	M	CLL	Subsequent treatment strategy	IV	Chemo, RT
72	M	NHL	Subsequent treatment strategy	III	Surgery, chemo
54	F	Breast	Subsequent treatment strategy	III	Surgery, chemo, RT
48	F	NHL	Subsequent treatment strategy	II	Chemo, RT
71	F	Breast	Subsequent treatment strategy	I	Surgery, chemo, RT
71	M	Lung	Initial treatment strategy	IV	None
65	M	NHL	Subsequent treatment strategy	IV	Chemo, RT
82	F	Breast	Subsequent treatment strategy	II	Surgery, chemo, RT
58	M	Bladder	Subsequent treatment strategy	II	Surgery, chemo
76	F	NHL	Subsequent treatment strategy	I	Chemo, RT
73	M	Sarcoma	Subsequent treatment strategy	II	Chemo, RT
72	F	NHL	Initial treatment strategy	II	None
27	F	NHL	Subsequent treatment strategy	I	Chemo
58	F	Pancreas	Subsequent treatment strategy	II	Surgery, chemo, RT
75	F	Rectum	Subsequent treatment strategy	III	Chemo, RT
63	M	NHL	Subsequent treatment strategy	IV	Chemo
55	F	Breast	Subsequent treatment strategy	III	Surgery, chemo, RT
74	M	NHL	Subsequent treatment strategy	III	Chemo
41	F	NHL	Subsequent treatment strategy	III	Chemo
86	M	NHL	Subsequent treatment strategy	I	Chemo, RT
34	F	Sarcoma	Subsequent treatment strategy	IV	Chemo
51	M	Colorectal	Subsequent treatment strategy	IV	Surgery, chemo, RT
39	M	NHL	Subsequent treatment strategy	IV	Chemo, RT

Clin Nucl Med. Author manuscript; available in PMC 2019 January 04.

Age	Sex	Cancer	Indication	Stage	Treatment
70	M	NHL	Subsequent treatment strategy	IV	Chemo
59	M	NHL	Subsequent treatment strategy	IV	Chemo
46	M	NHL	Subsequent treatment strategy	IV	Chemo
53	M	Lung	Subsequent treatment strategy	I	Surgery
69	M	Mesotdelioma	Subsequent treatment strategy	III	Surgery, chemo, RT
64	M	Sarcoma	Subsequent treatment strategy	IV	Surgery, chemo, RT
39	F	NHL	Subsequent treatment strategy	II	Chemo, RT
37	F	H&N SCC	Subsequent treatment strategy	II	Chemo, RT

NHL (non-Hodgkin lymphoma); HD (Hodgkin disease); CLL (chronic lymphocytic leukemia); RT (radiation therapy); H&N (head and neck); SCC (squamous cell carcionoma).

TABLE 2.

Details of SUV_{max} Measurements (±SD) in Normal Tissues

	PET/CT (non-TOF)	PET/MRI (TOF)	% Change	*P* Value
Cerebellum (*n* = 36)	10.6 ± 2.3	9.2 ± 2.1	−12.8 ± 9.3	0.0001
Parotid gland (*n* = 36)	2.2 ± 0.7	2.3 ± 0.7	6.7 ± 16.5	0.0344
Aortic arch (*n* = 34)	2.0 ± 0.5	1.1 ± 0.4	−45.4 ± 21.8	0.0001
Normal lung (*n* = 35)	0.6 ± 0.2	0.4 ± 0.1	−32.8 ± 17.4	0.0001
Liver (*n* = 34)	3.2 ± 0.6	2.3 ± 0.7	−26.4 ± 16.6	0.0001
Spleen (*n* = 30)	2.5 ± 0.9	2.2 ± 1.1	−12.5 ± 16.2	0.0013
Gluteal muscle (*n* = 33)	0.9 ± 0.3	1.2 ± 0.4	24.1 ± 31.2	0.0004
Gluteal fat (*n* = 33)	0.3 ± 0.1	0.2 ± 0.1	−3.4 ± 33.3	0.2698

Four patients had history of prior splenectomy. Two patients only had the head & neck acquisition of tde PET/MRI and 1 patient only had tde head & neck and chest acquisition of tde PET/MRI.

TABLE 3.

Details of SUV_{max} Measurements in Lesions (all Patients Included) Obtained From Non-TOF PET/CT Data

Discovery 600 and 690 vs. PET/MRI	**PET/CT (Non-TOF)**	**PET/MRI (TOF)**	**% Change**	***P* Value**
All lesions (*n* = 69)	6.5 ± 5.2	7.4 ± 5.3	21.0 ± 24.7	0.0001
Lymph nodes (*n* = 38)	6.7 ± 5.7	7.8 ± 6.2	23.8 ± 24.2	0.0001
Lung lesions (*n* = 9)	5.2 ± 4.4	5.7 ± 4.2	19.5 ± 25.0	0.0475
Bone lesions (*n* = 8)	9.0 ± 6.8	9.3 ± 5.1	18.3 ± 35.8	0.6631
Other lesions (*n* = 14)	5.1 ± 2.2	6.0 ± 2.8	16.8 ± 19.2	0.0062
Discovery 600 vs. PET/MRI	**PET/CT (non-TOF)**	**PET/MRI (TOF)**	**% Change**	***P* value**
All lesions (*n* = 16)	4.0 ± 1.9	4.9 ± 2.6	18.7 ± 27.3	0.0011
Lymph nodes (*n* = 10)	4.6 ± 2.1	6.0 ± 2.6	34.9 ± 21.0	0.0003
Lung lesions (*n* = 2)	2.4 ± 1.6	3.2 ± 1.4	44.6 ± 34.8	N/A
other lesions (*n* = 4)	3.2 ± 0.8	3.1 ± 1.1	−7.0 ± 11.7	0.4231
Discovery 690 vs. PET/MRI	**PET/CT (non-TOF)**	**PET/MRI (TOF)**	**% Change**	***P* value**
All lesions (*n* = 53)	7.2 ± 5.6	8.1 ± 5.8	19.4 ± 24.3	0.0001
Lymph nodes (*n* = 28)	7.5 ± 6.4	8.5 ± 7.0	19.8 ± 24.4	0.0015
Lung lesions (*n* = 7)	6.0 ± 4.7	6.5 ± 4.5	12.4 ± 19.0	0.1717
Bone lesions (*n* = 8)	9.0 ± 6.8	9.3 ± 5.1	18.3 ± 35.8	0.6631
other lesions (*n* = 10)	5.9 ± 2.2	7.2 ± 2.4	24.1 ± 17.6	0.0031

Clin Nucl Med. Author manuscript; available in PMC 2019 January 04.

TABLE 4.

Details of SUV_{max} Measurements Only in Lesions From Patients Scanned Using GE Discovery 690 With TOF (n = 15)

Discovery 690	**PET/CT (TOF)**	**PET/CT (Non-TOF)**	**% Change**	***P* Value**
All lesions (*n* = 26)	7.9 ± 5.0	8.0 ± 6.1	−3.2 ± 12.9	0.7403
Lymph nodes (*n* = 10)	7.8 ± 6.0	8.1 ± 7.3	−1.2 ± 14.8	0.4867
Lung lesions (*n* = 5)	6.4 ± 4.8	5.9 ± 4.6	−9.0 ± 6.7	0.0408
Bone lesions (*n* = 8)	8.6 ± 5.1	9.0 ± 6.8	−1.4 ± 15.3	0.6123
Otder lesions (*n* = 3)	8.3 ± 1.7	8.0 ± 2.1	−5.4 ± 7.7	0.3206
Discovery 690 vs. PET/MRI	**PET/CT (TOF)**	**PET/MRI (TOF)**	**% Change**	***P* value**
All lesions (*n* = 26)	7.9 ± 5.0	8.6 ± 6.1	10.2 ± 22.8	0.0575
Lymph nodes (*n* = 10)	7.8 ± 6.0	8.9 ± 8.3	9.5 ± 29.1	0.2860
Lung lesions (*n* = 5)	6.4 ± 4.8	6.6 ± 4.5	5.5 ± 13.6	0.5324
Bone lesions (*n* = 8)	8.6 ± 5.1	9.3 ± 5.1	13.5 ± 23.4	0.0951
Otder lesions (*n* = 3)	8.3 ± 1.7	9.2 ± 1.2	11.7 ± 17.7	0.3450
Discovery 690 vs. PET/MRI	**PET/CT (non-TOF)**	**PET/MRI (TOF)**	**% Change**	***P* value**
All lesions (*n* = 26)	8.0 ± 6.1	8.6 ± 6.1	16.2 ± 30.33	0.0609
Lymph nodes (*n* = 10)	8.1 ± 7.3	8.9 ± 8.3	13.1 ± 33.9	0.2814
Lung lesions (*n* = 5)	5.9 ± 4.6	6.6 ± 4.5	16.8 ± 20.8	0.0729
Bone lesions (*n* = 8)	9.0 ± 6.8	9.3 ± 5.1	18.3 ± 35.8	0.6631
Otder lesions (*n* = 3)	8.0 ± 2.1	9.2 ± 1.2	19.7 ± 29.8	0.3374

TABLE 5.

Details of Measured Radiation Dosage From PET and CT (Done Only for Attenuation Correction)

#	^{18}F FDG Dosage (mCi)	PET Dose (mSv)	CT Dose (mSv)
1	9.4	10.3	3.04
2	9.7	10.7	1.99
3	10.8	11.9	11.72
4	9.4	10.34	2.69
5	7.9	8.7	1.89
6	9.7	10.7	4.26
7	9.5	10.5	3.24
8	11.5	12.6	2.69
9	10.2	11.2	6.72
10	10.7	11.8	6.05
11	10.4	11.4	7.59
12	9.6	10.6	4.34
13	10.2	11.2	6.17
14	11.5	12.6	3.25
15	9.5	10.5	6.26
16	11.8	12.9	3.84
17	9.7	10.7	3.36
18	9.0	9.9	5.33
19	9.9	10.9	1.24
20	10.6	11.7	5.19
21	11.2	12.3	2.68
22	11.5	12.6	6.43
23	11.2	12.3	4.19
24	8.7	9.6	3.25
25	11.00	12.10	7.24
26	9.10	10.01	15.05
27	10.80	11.88	8.53
28	10.80	11.88	6.52
29	10.40	11.44	6.56
30	10.60	11.66	9.39
31	9.50	10.45	10.44
32	9.70	10.67	2.12
33	10.50	11.55	9.44
34	10.00	11.00	7.89
35	9.00	9.90	11.33
36	9.50	10.45	4.67